

Quantum-embedding description of the Anderson lattice model with the ghost Gutzwiller Approximation

Marius S. Frank,¹ Tsung-Han Lee,² Gargee Bhattacharyya,¹ Pak Ki Henry Tsang,³
Victor L. Quito,^{4,3} Vladimir Dobrosavljević,³ Ove Christiansen,⁵ and Nicola Lanata^{1,6,*}

¹*Department of Physics and Astronomy, Aarhus University, 8000, Aarhus C, Denmark*

²*Physics and Astronomy Department, Rutgers University, Piscataway, New Jersey 08854, USA*

³*Department of Physics and National High Magnetic Field Laboratory,
Florida State University, Tallahassee, Florida 32306, USA*

⁴*Department of Physics and Astronomy, Iowa State University, Ames, Iowa 50011, USA*

⁵*Department of Chemistry, Aarhus University, 8000, Aarhus C, Denmark*

⁶*Nordita, KTH Royal Institute of Technology and Stockholm University,
Hannes Alfvéns väg 12, SE-106 91 Stockholm, Sweden*

(Dated: July 27, 2021)

We present benchmark calculations of the Anderson lattice model based on the recently-developed “ghost Gutzwiller approximation”. Our analysis shows that, in some parameters regimes, the predictions of the standard Gutzwiller approximation can be incorrect by orders of magnitude for this model. We show that this is caused by the inability of this method to describe simultaneously the Mott physics and the hybridization between correlated and itinerant degrees of freedom —whose interplay often governs the metal-insulator transition in real materials. Finally, we show that the ghost Gutzwiller approximation solves this problem, providing us with results in remarkable agreement with dynamical mean field theory throughout the entire phase diagram, while being much less computationally demanding. We provide an analytical explanation of these findings and discuss their implications within the context of ab-initio computation of strongly-correlated matter.

Understanding and simulating quantitatively the electronic behavior of strongly correlated matter is one of the most fundamental problems in condensed-matter science. The substantial progress achieved today in this direction largely owes to quantum embedding methods [1, 2]. In particular, the development of dynamical mean field theory (DMFT) [3–13] constituted a great leap in our understanding of strong-correlation phenomena, which advanced dramatically our ability of describing the properties of real materials. In the past decade, the perspective of expanding the predictive power of simulations within the blooming field of theory-assisted materials-by-design [14, 15] contributed to stimulate the development of alternative computational frameworks, capable of taking into account strong correlations at a lower computational cost. Within this context, particularly promising approaches are the Gutzwiller approximation (GA) [16–21] —or, equivalently [22, 23], the rotationally-invariant slave-boson mean-field theory [24–26] — and density matrix embedding theory [27, 28]. These frameworks have similar algorithmic structures. In fact, as in density matrix embedding theory, the GA equations can be cast in terms of ground-state calculations of auxiliary impurity models called embedding Hamiltonians (EH), where the bath has the same number of degrees of freedom as the impurity [20]. Furthermore, density matrix embedding theory can be formally derived from the GA equations, setting to unity the parameters encoding the quasi-particle mass-renormalization weights [29, 30]. More recently, a more accurate extension of the GA, called “ghost Gutzwiller approximation” (g-GA) has been de-

veloped [31], based on the idea of extending the GA variational space introducing auxiliary (ghost) fermionic degrees of freedom.

Here we present benchmark calculations of the Anderson lattice model (ALM) and demonstrate that, by construction, the GA cannot capture the interplay between Mott physics and the hybridization between correlated and itinerant degrees of freedom —which generally coexist and whose interplay often governs the metal-insulator transition in real materials. We also show that, in some parameters regimes, this limitation of the GA can result in overestimating the Mott critical point by orders of magnitude. Finally, we demonstrate, both numerically and analytically, that the g-GA method resolves these problems, while remaining much less computationally demanding than DMFT. Furthermore, we show that this method allows us to describe semi-analytically the spectral properties (both at low and high energies) throughout the entire phase diagram of the ALM, facilitating the physical interpretation of the numerical results.

Model.— We consider the ALM on a Bethe lattice, in the limit of infinite coordination number [32]:

$$\begin{aligned} \hat{H} &= \sum_{\langle i,j \rangle} \sum_{\sigma} (t_{ij} + \delta_{ij} \epsilon_p) p_{i\sigma}^{\dagger} p_{j\sigma} + \sum_i \frac{U}{2} (\hat{n}_{di} - 1)^2 \\ &+ V \sum_{i\sigma} (p_{i\sigma}^{\dagger} d_{i\sigma} + \text{H.c.}) - \mu \sum_i \hat{N}_i \\ &= \sum_{k\sigma} \sum_{\alpha\beta} [\tau_k]_{\alpha\beta} [\phi_{k\sigma}^{\dagger}]_{\alpha} [\phi_{k\sigma}]_{\beta} + U \sum_i d_{i\uparrow}^{\dagger} d_{i\uparrow} d_{i\downarrow}^{\dagger} d_{i\downarrow}, \end{aligned} \quad (1)$$

where: $p_{i\sigma}$ and $d_{i\sigma}$ are Fermionic annihilation operators, $p_{i\sigma}^\dagger$ and $d_{i\sigma}^\dagger$ are Fermionic creation operators, i and j are site labels, σ is the spin, $\langle i, j \rangle$ indicates that the corresponding summation is restricted to first nearest neighbours, the hopping matrix t_{ij} is uniform, μ is the chemical potential, $\hat{n}_{di} = \sum_{\sigma} d_{i\sigma}^\dagger d_{i\sigma}$, $\hat{n}_{pi} = \sum_{\sigma} p_{i\sigma}^\dagger p_{i\sigma}$, $\hat{N}_i = \hat{n}_{di} + \hat{n}_{pi}$, $\phi_{k\sigma}^\dagger = (p_{k\sigma}^\dagger, d_{k\sigma}^\dagger)$, $\phi_{k\sigma} = \sum_i \mathcal{U}_{ik} \phi_{i\sigma}^\dagger$,

$$\tau_k = \begin{pmatrix} \epsilon_k + \epsilon_p - \mu & V \\ V & -U/2 - \mu \end{pmatrix}, \quad (2)$$

the columns of \mathcal{U} are the eigenvectors of t and ϵ_k are its eigenvalues. From now on we fix the hopping matrix t by using the half-bandwidth of ϵ_k (corresponding to a semi-circular density of states) as the energy unit.

Method.— Here we summarize the algorithmic structure of the g-GA and the GA, pointing out the key differences between these two methods, from a quantum-embedding perspective [20, 26, 31]. For simplicity, below we focus on the ALM introduced above, while the general theory for arbitrary multi-orbital systems is summarized in the supplemental material [33]. For both the g-GA and the GA, the solution is obtained by calculating recursively the *ground state* of 2 auxiliary systems: (1) the so-called “quasiparticle Hamiltonian” (QPH) and (2) the “embedding Hamiltonian” (EH).

The EH can be expressed in the following form:

$$\begin{aligned} \hat{\mathcal{H}}_{\text{emb}}^{\text{g-GA}} &= \frac{U}{2} (\hat{n}_d - 1)^2 - \mu \hat{n}_d + \sum_{\sigma} \sum_{a,b=1}^B \lambda_{ab}^c \hat{f}_{b\sigma} \hat{f}_{a\sigma}^\dagger \\ &+ \sum_{a=1}^B \sum_{\sigma} D_a \left(\hat{d}_{\sigma}^\dagger \hat{f}_{a\sigma} + \text{H.c.} \right) \end{aligned} \quad (3)$$

$$\begin{aligned} \hat{\mathcal{H}}_{\text{emb}}^{\text{GA}} &= \frac{U}{2} (\hat{n}_d - 1)^2 - \mu \hat{n}_d + \sum_{\sigma} \lambda^c \hat{f}_{\sigma} \hat{f}_{\sigma}^\dagger \\ &+ \sum_{\sigma} D \left(\hat{d}_{\sigma}^\dagger \hat{f}_{\sigma} + \text{H.c.} \right), \end{aligned} \quad (4)$$

where the \hat{d} operators correspond to the EH impurity

degrees of freedom, $\hat{n}_d = \sum_{\sigma} \hat{d}_{\sigma}^\dagger \hat{d}_{\sigma}$, the \hat{f} operators correspond to the EH bath degrees of freedom and the parameters D and λ^c are determined self-consistently [33]. Note that, while in standard GA the bath of the EH has the same size of the impurity, within the g-GA it contains a larger number of sites ($B > 1$). As in Refs. [31, 34], here we will set $B = 3$ (the effect of increasing B , which would enlarge further the variational space, will be subject of future work). After convergence, the expectation value of any local operator $\hat{O}[d_{i\alpha}^\dagger, d_{i\alpha}]$ can be calculated from the ground state $|\Phi\rangle$ of the EH as:

$$\langle \hat{O} \rangle = \langle \Phi | \hat{O}[d_{i\alpha}^\dagger, d_{i\alpha}] | \Phi \rangle. \quad (5)$$

The QPH can be expressed as:

$$\begin{aligned} \hat{\mathcal{H}}_{\text{qp}}^{\text{g-GA}} &= \sum_{i\sigma} \sum_{a=1}^B l_a f_{i\sigma}^\dagger f_{i\sigma} \\ &+ \sum_{i\sigma} \sum_{a=1}^B V(r_a f_{i\sigma}^\dagger p_{i\sigma} + \text{H.c.}) \\ &+ \sum_{i\sigma} (\epsilon_p - \mu) p_{i\sigma}^\dagger p_{i\sigma} + \sum_{ij\sigma} t_{ij} p_{i\sigma}^\dagger p_{j\sigma} \end{aligned} \quad (6)$$

$$\begin{aligned} \hat{\mathcal{H}}_{\text{qp}}^{\text{GA}} &= \sum_{i\sigma} l f_{i\sigma}^\dagger f_{i\sigma} + \sum_{i\sigma} V(r f_{i\sigma}^\dagger p_{i\sigma} + \text{H.c.}) \\ &+ \sum_{i\sigma} (\epsilon_p - \mu) p_{i\sigma}^\dagger p_{i\sigma} + \sum_{ij\sigma} t_{ij} p_{i\sigma}^\dagger p_{j\sigma}, \end{aligned} \quad (7)$$

where the $f_{i\sigma}$ operators are “quasiparticle modes” residing in an auxiliary (enlarged) Hilbert space [33]. Once the parameters l and r are determined self-consistently in the form above [33], the resulting Green’s function for the modes $\phi_{k\sigma}$ is:

$$\mathcal{G}(k, \omega) = [\omega - \tau_k - \Sigma(\omega)]^{-1}, \quad (8)$$

where the only non-zero entry of $\Sigma(\omega)$ is the dd component, which is given by the following equations:

$$\Sigma_{dd}^{\text{g-GA}}(\omega) = \mu + \frac{U}{2} + \frac{l_1}{r_1^2} - \omega \frac{1-r_1^2}{r_1^2} + \frac{(\omega-l_1)^2}{r_1^4} [(\omega-l_3)r_2^2 + (\omega-l_2)r_3^2] \left[(\omega-l_2)(\omega-l_3) + \frac{\omega-l_1}{r_1^2} (r_2^2(\omega-l_3) + r_3^2(\omega-l_2)) \right]^{-1} \quad (9)$$

$$\Sigma_{dd}^{\text{GA}}(\omega) = \mu + \frac{U}{2} + \frac{l}{r^2} - \omega \frac{1-r^2}{r^2}. \quad (10)$$

As demonstrated in the supplemental material [33] (and shown in the calculations below): (i) the poles of $\mathcal{G}(k, \omega)$ are located on top of the eigenvalues of the corresponding QPHs [35–38], and (ii) the resulting total spec-

tral weight of the d degrees of freedom is given by:

$$\int_{-\infty}^{\infty} \mathcal{A}_{dd}^{\text{g-GA}}(k, \omega) d\omega = \sum_{a=1}^B r_a^2 \quad (11)$$

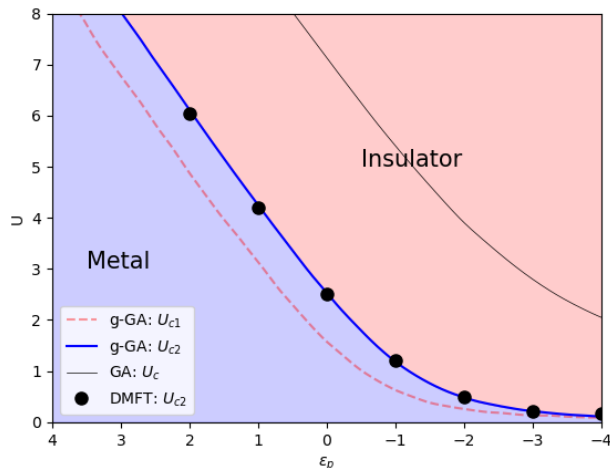


Figure 1. Paramagnetic phase diagram of the ALM on an infinite-coordination Bethe lattice, for 3 electrons per site and $V = 1$. The g-GA metal-insulator transition U_{c2} and the end of the metal-insulator coexistence region U_{c1} are marked in blue and red, respectively. The black dots are U_{c2} values calculated with DMFT+CTQMC, at $T = 0.01$. The gray line indicates the metal-insulator transition in bare GA.

$$\int_{-\infty}^{\infty} \mathcal{A}_{dd}^{\text{GA}}(k, \omega) d\omega = r^2, \quad (12)$$

where $\mathcal{A}_{dd}^{\text{g-GA}}$ and $\mathcal{A}_{dd}^{\text{GA}}$ are the g-GA and GA d -electron spectral functions, respectively, and r^2 is the GA d -electron quasiparticle weight [39]. From the parameters R, λ and the ground state $|\Psi_0\rangle$ of the corresponding QPH, it is also possible to calculate the expectation values of all non-local quadratic operators. In particular:

$$\langle d_{i\sigma}^\dagger p_{i\sigma} \rangle_{\text{g-GA}} = \sum_{a=1}^B r_a \langle \Psi_0 | f_{ia\sigma}^\dagger p_{i\sigma} | \Psi_0 \rangle \quad (13)$$

$$\langle d_{i\sigma}^\dagger p_{i\sigma} \rangle_{\text{GA}} = r \langle \Psi_0 | f_{i\sigma}^\dagger p_{i\sigma} | \Psi_0 \rangle. \quad (14)$$

For completeness, the generalization of all analytical results listed above to arbitrary multi-orbital systems is given in the supplemental material [33].

Results.— In Fig. 1 we show the g-GA phase diagram of the ALM (in the paramagnetic phase) for total occupancy $\langle \hat{N}_i \rangle = 3$. The g-GA results are compared with DMFT—with the continuous time quantum Monte Carlo (CTQMC) impurity solver [40–42], at temperature $T = 0.01$ — and with the bare GA. Our benchmark calculations show that the g-GA phase diagram is consistent with previous work [43–45] and in remarkable agreement with DMFT. As expected, both the g-GA method and the bare GA capture the fact that the Mott metal-insulator transition point U_{c2} vanishes for $\epsilon_p \rightarrow -\infty$ —corresponding to the limit where the p degrees of freedom are gapped out. However, the interaction U_c of the metal-insulator transition is largely overestimated within the GA, especially for $\epsilon_p \ll -1$. Note that the phase di-

agram for $\langle \hat{N}_i \rangle = 1$ can be automatically inferred from our calculations above, as they are related to each other by a particle-hole transformation.

In Fig. 2 we show the behavior of the g-GA total energy \mathcal{E} , the occupancies $n_p = \langle \hat{n}_{pi} \rangle$ and $n_d = \langle \hat{n}_{di} \rangle$, the d -electron double occupancy $D = \langle \hat{n}_{di\uparrow} \hat{n}_{di\downarrow} \rangle$, the p - d “hybridization energy” $H = \sum_{\sigma} \langle d_{i\sigma}^\dagger p_{i\sigma} \rangle + \text{c.c.}$, and the d -electron quasiparticle weight:

$$\begin{aligned} Z &= \left[1 - \frac{\partial \Sigma^{\text{g-GA}}}{\partial \omega} \right]_{\omega=0}^{-1} \\ &= \frac{(l_2 l_3 r_1^2 + l_1 l_3 r_2^2 + l_1 l_2 r_3^2)^2}{l_1^2 l_3^2 r_2^2 + l_2^2 (l_3^2 r_1^2 + l_1^2 r_3^2)}. \end{aligned} \quad (15)$$

The g-GA results are shown in comparison with the bare GA and DMFT. While the GA solution is considered accurate only for weak interactions, we find that the agreement between g-GA and DMFT is remarkable for all observables, in all parameters regimes.

Let us now analyze the single-particle Green’s function. In Fig. 3 we consider $\epsilon_p = -1$ and 3 values of U , showing the total g-GA energy-resolved spectral function:

$$\mathcal{A}(k, \omega) = -\frac{1}{\pi} \text{ImTr}[\mathcal{G}(k, \omega)] \quad (16)$$

and the p and d local density of states. The DMFT spectra were obtained by performing analytical continuation with the maximum entropy method [46]. Interestingly, the g-GA captures systematically the main features of the DMFT spectra (including the Hubbard bands, and the hybridization between the p and d degrees of freedom). Note that, to interpret the behavior of the g-GA spectra, it is possible to exploit its relation with the bands of the QPH [Eq. (6)], previously discussed in the methods section. In particular, the relative position of the p band with respect to the Fermi level is approximately encoded in the corresponding on-site energy $\epsilon_p^* = \epsilon_p - \mu$, while the positions of the d -electron low-energy and high-energy excitations are approximately encoded in the variational parameters l_a ($a = 1, 2, 3$).

A key fact emerging from our benchmark calculations is that the GA can overestimate U_c dramatically (especially for $\epsilon_p \ll -1$), see Fig. 1. To explain this result we note that, by construction, the GA Mott transition occurs when the quasiparticle weight $Z = r^2$ vanishes, see Eq. (10). Therefore, the corresponding approximation to the Mott phase is such that $\langle d_{i\sigma}^\dagger p_{i\sigma} \rangle_{\text{GA}} = 0$, see Eq. (14). In other words, this method cannot describe simultaneously the Mott phase and the p - d charge fluctuations. But this is unrealistic for the ALM, where the p - d hybridization effects are generally very large, not only in the weakly-interacting regime, but also for $U \simeq U_{c2}$ and $U > U_{c2}$, see Figs. 2,3. Because of the variational principle, this results in a systematic overestimation of the total energy as we approach the Mott phase (see Fig. 2),

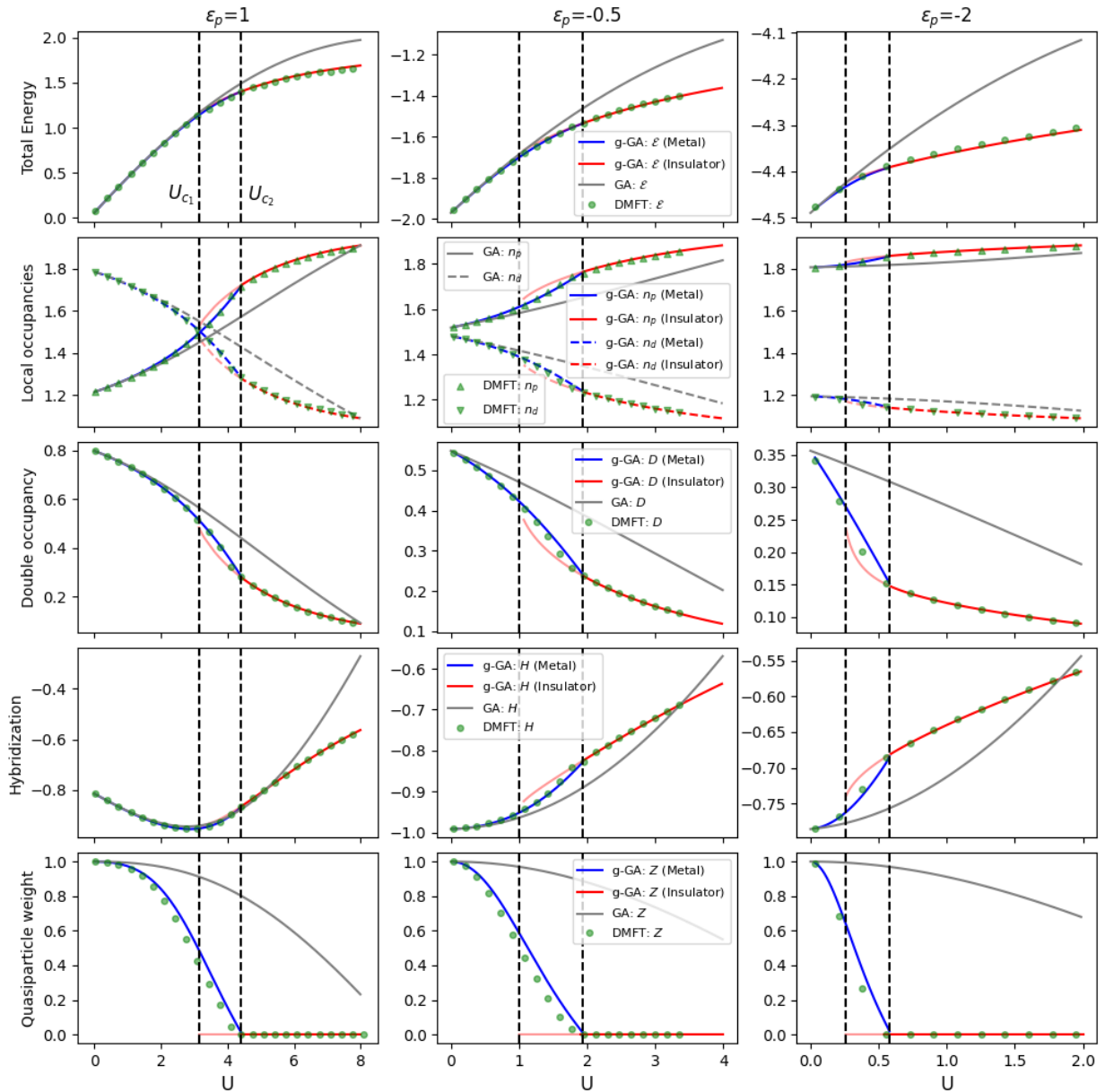


Figure 2. Behavior of the g-GA total energy \mathcal{E} , local occupancies $n_p = \langle \hat{n}_{pi} \rangle$ and $n_d = \langle \hat{n}_{di} \rangle$, d -electron double occupancy $D = \langle \hat{n}_{di\uparrow} \hat{n}_{di\downarrow} \rangle$, p - d hybridization $H = \sum_{\sigma} \langle d_{i\sigma}^{\dagger} p_{i\sigma} \rangle + \text{c.c.}$ and d -electron quasiparticle weight Z , for the ALM on an infinite- d -coordination Bethe lattice, in comparison with DMFT and the bare GA. The DMFT data are computed with CTQMC, at $T = 0.01$ for $\epsilon_p = 1$ and $\epsilon_p = -0.5$ and at $T = 0.02$ for $\epsilon_p = -2$. The vertical black dashed lines indicate U_{c1} and U_{c2} .

causing an overestimation of the metal-insulator transition point. This point is documented in further detail in the supplemental material, where the GA overestimation of U_c at $\epsilon_p \ll -1$ is explained in relation to a qualitative pathological behavior of the GA variational parameter r in the narrow-bandwidth limit ($t \rightarrow 0$).

Remarkably, since the g-GA captures the existence of

the Hubbard bands, the right side of Eq. (11) never vanishes [31]. Therefore, similar to DMFT, $\langle d_{i\sigma}^{\dagger} p_{i\sigma} \rangle_{\text{g-GA}}$ remains finite even in the Mott phase (see Eq. (13)). This shows that the ability of the g-GA of describing simultaneously the Mott physics and the d - p hybridization is directly connected with its ability of describing the transfer of d -electron spectral weight to the Hubbard bands

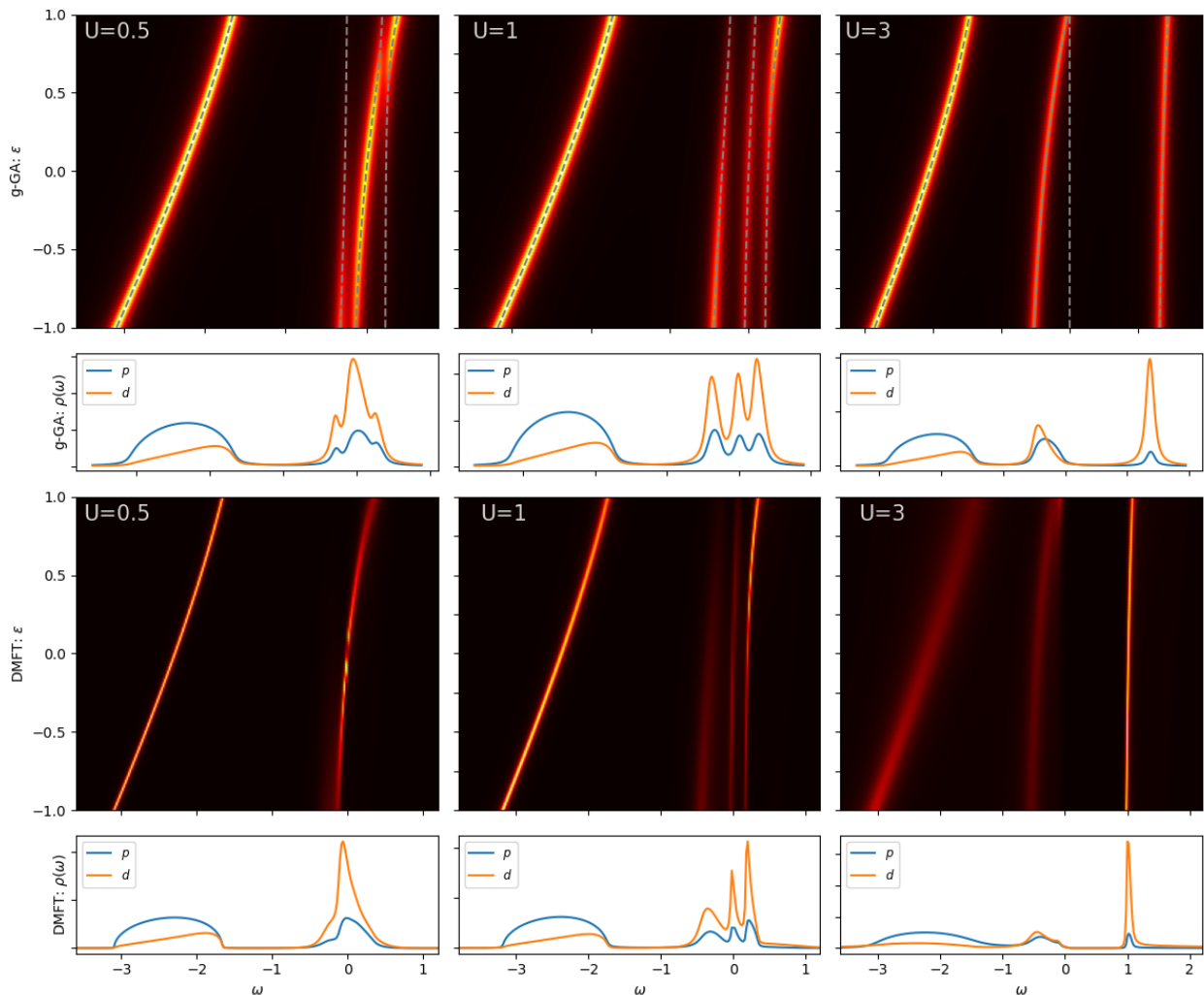


Figure 3. Energy-resolved spectral function and corresponding p and d local density of states $\rho(\omega)$, calculated with g-GA (upper panels) and DMFT+CTQMC (lower panels), for $\epsilon_p = -1$ and 3 values of U . The g-GA spectra is visualized using a small artificial smearing, $\Gamma = 0.06$. The g-GA quasiparticle bands are indicated by gray dashed lines.

(which the bare GA lacks).

Conclusions.— We performed benchmark calculations of the ALM, showing that the g-GA provides us with results with accuracy comparable to DMFT, both for the ground-state and the spectral properties. In particular, we showed that the g-GA is capable of describing accurately the interplay between the Mott physics and the hybridization between correlated and itinerant degrees of freedom, while the GA cannot describe simultaneously these effects. This is particularly relevant for real-material calculations in combination with density functional theory [17, 20, 47, 48], where the correlated orbitals are generally very localized around their atomic positions [49, 50]—so that the interactions with their environment are mainly mediated by the itinerant modes (as in the ALM studied here). In fact, it is well possible

that the limitation of the GA here uncovered explains why, in some cases, simulating the properties of real materials with the GA requires to use unphysically-large Hubbard U [51], and suggests that multi-orbital implementations of the g-GA will resolve these problems.

From the computational standpoint, the g-GA is more expensive than the bare GA (as the bath of the EH contains additional degrees of freedom). On the other hand, its computational complexity remains much lower than DMFT. In fact, the g-GA requires to calculate only the ground state of a finite-size impurity model (while in DMFT it is necessary to calculate the spectra of an impurity model with an infinite bath). For example, in our DMFT calculations each CTQMC iteration (performed using 5×10^8 Monte Carlo steps, in parallel, on 72 cores) required about 2 minutes of computational time. In-

stead, within our g-GA calculations each EH iteration (performed on a single core) required about 0.2-0.3 seconds. Note also that the difference in computational complexity between DMFT and g-GA grows exponentially as a function of the impurity size.

A particularly promising perspective is the possibility of solving the g-GA equations with hybrid quantum-classical frameworks [52], employing impurity solvers based on quantum algorithms such as variational quantum eigensolvers [53–56]. In fact, within the g-GA, realizing such program for real-material applications may require devices consisting of only tens of qubits, while it has been estimated that quantum computers with at least 100 logical qubits will be necessary for applications within DMFT [57]. Furthermore, since the number of parameters characterizing the EH is finite, the recently-developed approach based on machine learning for the GA [58] will be applicable also to the g-GA, as we hope to show in future work. Note also that the g-GA can be equivalently formulated in terms of the rotationally-invariant slave-boson mean-field theory [31], which is based on an exact reformulation of the many-body problem. This line of interpretation may open the possibility of developing beyond-mean-field schemes, providing us with new routes for high-precision calculations.

ACKNOWLEDGEMENTS

We thank Gabriel Kotliar for useful discussions. We gratefully acknowledge funding from the Novo Nordisk Foundation through the Exploratory Interdisciplinary Synergy Programme project NNF19OC0057790. We thank support from the VILLUM FONDEN through the Villum Experiment project 00028019 and the Centre of Excellence for Dirac Materials (Grant. No. 11744). T.-H.L. was supported by the Computational Materials Sciences Program funded by the US Department of Energy, Office of Science, Basic Energy Sciences, Materials Sciences and Engineering Division. Work in Florida was supported by the NSF Grant No. 1822258, and the National High Magnetic Field Laboratory through the NSF Cooperative Agreement No. 1157490 and the State of Florida.

* Corresponding author: lanata@phys.au.dk

- [1] P. R. C. Kent and G. Kotliar, Toward a predictive theory of correlated materials, *Science* **361**, 348 (2018).
- [2] Q. Sun and G.-K.-L. Chan, Quantum embedding theories, *Acc. Chem. Res.* **49**, 2705 (2016).
- [3] A. Georges, G. Kotliar, W. Krauth, and M. J. Rozenberg, Dynamical mean-field theory of strongly correlated fermion systems and the limit of infinite dimensions, *Rev. Mod. Phys.* **68**, 13 (1996).
- [4] V. Anisimov and Y. Izyumov, *Electronic Structure of Strongly Correlated Materials* (Springer, 2010).
- [5] T. Maier, M. Jarrell, T. Pruschke, and M. H. Hettler, Quantum cluster theories, *Rev. Mod. Phys.* **77**, 1027 (2005).
- [6] G. Kotliar, S. Y. Savrasov, G. Pálsson, and G. Biroli, Cellular dynamical mean field approach to strongly correlated systems, *Phys. Rev. Lett.* **87**, 186401 (2001).
- [7] A. I. Lichtenstein and M. I. Katsnelson, Antiferromagnetism and *d*-wave superconductivity in cuprates: A cluster dynamical mean-field theory, *Phys. Rev. B* **62**, R9283 (2000).
- [8] M. Potthoff, M. Aichhorn, and C. Dahnken, Variational cluster approach to correlated electron systems in low dimensions, *Phys. Rev. Lett.* **91**, 206402 (2003).
- [9] D. Senechal, D. Perez, and M. Pioro-Ladriere, The spectral weight of the Hubbard model through cluster perturbation theory, *Phys. Rev. Lett.* **84**, 522 (2000).
- [10] M. Aichhorn, L. Pourovskii, V. Vildosola, M. Ferrero, O. Parcollet, T. Miyake, A. Georges, and S. Biermann, Dynamical mean-field theory within an augmented plane-wave framework: Assessing electronic correlations in the iron pnictide LaFeAsO, *Phys. Rev. B* **80**, 085101 (2009).
- [11] G. Kotliar, S. Y. Savrasov, K. Haule, V. S. Oudovenko, O. Parcollet, and C. A. Marianetti, Electronic structure calculations with dynamical mean-field theory, *Rev. Mod. Phys.* **78**, 865 (2006).
- [12] K. Held, A. Nekrasov, G. Keller, V. Eyert, N. Blümer, A. K. McMahan, R. T. Scalettar, T. Pruschke, V. I. Anisimov, and D. Vollhardt, Realistic investigations of correlated electron systems with LDA+DMFT, *Phys. Stat. Sol. (B)* **243**, 2599 (2006).
- [13] J.-Z. Zhao, J.-N. Zhuang, X.-Y. Deng, Y. Bi, L.-C. Cai, Z. Fang, and X. Dai, Implementation of LDA+DMFT with the pseudo-potential-plane-wave method, *Chin. Phys. B* **21**, 057106 (2012).
- [14] L.-Q. Chen, L.-D. Chen, S. V. Kalinin, G. Klimeck, S. K. Kumar, J. Neugebauer, and I. Terasaki, Design and discovery of materials guided by theory and computation, *npj Computational Materials* **1**, 15007 (2015).
- [15] R. Adler, C.-J. Kang, C.-H. Yee, and G. Kotliar, Correlated materials design: prospects and challenges, *Reports on Progress in Physics* **82**, 012504 (2018).
- [16] M. C. Gutzwiller, Correlation of Electrons in a Narrow *s* Band, *Phys. Rev.* **137**, A1726 (1965).
- [17] X.-Y. Deng, L. Wang, X. Dai, and Z. Fang, Local density approximation combined with Gutzwiller method for correlated electron systems: Formalism and applications, *Phys. Rev. B* **79**, 075114 (2009).
- [18] K. M. Ho, J. Schmalian, and C. Z. Wang, Gutzwiller density functional theory for correlated electron systems, *Phys. Rev. B* **77**, 073101 (2008).
- [19] T. Schickling, F. Gebhard, and J. Bünemann, Antiferromagnetic order in multiband Hubbard models for iron pnictides, *Phys. Rev. Lett.* **106**, 146402 (2011).
- [20] N. Lanatà, Y.-X. Yao, C.-Z. Wang, K.-M. Ho, and G. Kotliar, Phase diagram and electronic structure of praseodymium and plutonium, *Phys. Rev. X* **5**, 011008 (2015).
- [21] N. Lanatà, H. U. R. Strand, X. Dai, and B. Hellsing, Efficient implementation of the Gutzwiller variational method, *Phys. Rev. B* **85**, 035133 (2012).
- [22] J. Bünemann and F. Gebhard, Equivalence of Gutzwiller and slave-boson mean-field theories for multiband

- Hubbard models, Phys. Rev. B **76**, 193104 (2007).
- [23] N. Lanatà, P. Barone, and M. Fabrizio, Fermi-surface evolution across the magnetic phase transition in the Kondo lattice model, Phys. Rev. B **78**, 155127 (2008).
- [24] R. Frésard and P. Wölfle, Unified slave boson representation of spin and charge degrees of freedom for strongly correlated fermi systems, International Journal of Modern Physics B **06**, 685 (1992).
- [25] F. Lechermann, A. Georges, G. Kotliar, and O. Parcollet, Rotationally invariant slave-boson formalism and momentum dependence of the quasiparticle weight, Phys. Rev. B **76**, 155102 (2007).
- [26] N. Lanatà, Y.-X. Yao, X. Deng, V. Dobrosavljević, and G. Kotliar, Slave Boson Theory of Orbital Differentiation with Crystal Field Effects: Application to UO₂, Phys. Rev. Lett. **118**, 126401 (2017).
- [27] G. Knizia and G. K.-L. Chan, Density matrix embedding: A simple alternative to dynamical mean-field theory, Phys. Rev. Lett. **109**, 186404 (2012).
- [28] E. Fertitta and G. H. Booth, Rigorous wave function embedding with dynamical fluctuations, Phys. Rev. B **98**, 235132 (2018).
- [29] T. Ayral, T.-H. Lee, and G. Kotliar, Dynamical mean-field theory, density-matrix embedding theory, and rotationally invariant slave bosons: A unified perspective, Phys. Rev. B **96**, 235139 (2017).
- [30] T.-H. Lee, T. Ayral, Y.-X. Yao, N. Lanatà, and G. Kotliar, Rotationally invariant slave-boson and density matrix embedding theory: Unified framework and comparative study on the one-dimensional and two-dimensional Hubbard model, Phys. Rev. B **99**, 115129 (2019).
- [31] N. Lanatà, T.-H. Lee, Y.-X. Yao, and V. Dobrosavljević, Emergent Bloch excitations in Mott matter, Phys. Rev. B **96**, 195126 (2017).
- [32] W. Metzner and D. Vollhardt, Correlated lattice fermions in $d = \infty$ dimensions, Phys. Rev. Lett. **62**, 324 (1989).
- [33] Supplemental material: Lagrange formulation of the g-GA in multi-orbital case (including general analytical expression for the g-GA self energy) and details about GA pathology in narrow-band limit.
- [34] D. Guerci, M. Capone, and M. Fabrizio, Exciton Mott transition revisited, Phys. Rev. Materials **3**, 054605 (2019).
- [35] J. K. Jain and P. W. Anderson, Beyond the fermi liquid paradigm: Hidden fermi liquids, Proceedings of the National Academy of Sciences **106**, 9131 (2009).
- [36] S. Y. Savrasov, K. Haule, and G. Kotliar, Many-body electronic structure of americium metal, Phys. Rev. Lett. **96**, 036404 (2006).
- [37] S. Y. Savrasov, V. Oudovenko, K. Haule, D. Villani, and G. Kotliar, Interpolative approach for solving the Anderson impurity model, Phys. Rev. B **71**, 115117 (2005).
- [38] S. Sakai, M. Civelli, and M. Imada, Hidden-fermion representation of self-energy in pseudogap and superconducting states of the two-dimensional Hubbard model, Phys. Rev. B **94**, 115130 (2016).
- [39] J. Büneemann, F. Gebhard, and R. Thul, Landau-Gutzwiller quasiparticles, Phys. Rev. B **67**, 075103 (2003).
- [40] P. Werner, A. Comanac, L. de' Medici, M. Troyer, and A. J. Millis, Continuous-time solver for quantum impurity models, Phys. Rev. Lett. **97**, 076405 (2006).
- [41] E. Gull, A. J. Millis, A. I. Lichtenstein, A. N. Rubtsov, M. Troyer, and P. Werner, Continuous-time Monte Carlo methods for quantum impurity models, Rev. Mod. Phys. **83**, 349 (2011).
- [42] K. Haule, Quantum Monte Carlo impurity solver for cluster dynamical mean-field theory and electronic structure calculations with adjustable cluster base, Phys. Rev. B **75**, 155113 (2007).
- [43] A. Amaricci, L. de' Medici, and M. Capone, Mott transitions with partially filled correlated orbitals, EPL (Europhysics Letters) **118**, 17004 (2017).
- [44] J. Zaanen, G. A. Sawatzky, and J. W. Allen, Band gaps and electronic structure of transition-metal compounds, Phys. Rev. Lett. **55**, 418 (1985).
- [45] G. Sordi, A. Amaricci, and M. J. Rozenberg, Metal-insulator transitions in the periodic anderson model, Phys. Rev. Lett. **99**, 196403 (2007).
- [46] M. Jarrell and J. E. Gubernatis, Bayesian inference and the analytic continuation of imaginary-time quantum Monte Carlo data, Physics Reports **269**, 133 (1996).
- [47] V. I. Anisimov, A. I. Oteryaev, M. A. Korotin, A. O. Anokhin, and G. Kotliar, First-principles calculations of the electronic structure and spectra of strongly correlated systems: dynamical mean-field theory, J. Phys. Condens. Matter **9**, 7359 (1997).
- [48] V. I. Anisimov, F. Aryasetiawan, and A. I. Lichtenstein, First-principles calculations of the electronic structure and spectra of strongly correlated systems: the LDA+U method, J. Phys. Condens. Matter **9**, 767 (1997).
- [49] K. Haule, C.-H. Yee, and K. Kim, Dynamical mean-field theory within the full-potential methods: Electronic structure of CeIrIn₅, CeCoIn₅, and CeRhIn₅, Phys. Rev. B **81**, 195107 (2010).
- [50] F. Lechermann, A. Georges, A. Poteryaev, S. Biermann, M. Posternak, A. Yamasaki, and O. K. Andersen, Dynamical mean-field theory using Wannier functions: A flexible route to electronic structure calculations of strongly correlated materials, Phys. Rev. B **74**, 125120 (2006).
- [51] N. Lanatà, T.-H. Lee, Y.-X. Yao, V. Stevanović, and V. Dobrosavljević, Connection between Mott physics and crystal structure in a series of transition metal binary compounds, npj Comput. Mater. **5**, 30 (2019).
- [52] Y.-X. Yao, F. Zhang, C.-Z. Wang, K.-M. Ho, and P. P. Orth, Gutzwiller hybrid quantum-classical computing approach for correlated materials, Phys. Rev. Research **3**, 013184 (2021).
- [53] J. R. McClean, J. Romero, R. Babbush, and A. Aspuru-Guzik, The theory of variational hybrid quantum-classical algorithms, New Journal of Physics **18**, 023023 (2016).
- [54] P. J. J. O'Malley, R. Babbush, I. D. Kivlichan, J. Romero, J. R. McClean, R. Barends, J. Kelly, P. Roushan, A. Tranter, N. Ding, *et al.*, Scalable quantum simulation of molecular energies, Physical Review X **6**, 031007 (2016).
- [55] A. Kandala, A. Mezzacapo, K. Temme, M. Takita, M. Brink, J. M. Chow, and J. M. Gambetta, Hardware-efficient variational quantum eigensolver for small molecules and quantum magnets, Nature **549**, 242 (2017).
- [56] J. Romero, R. Babbush, J. R. McClean, C. Hempel, P. J. Love, and A. Aspuru-Guzik, Strategies for quantum computing molecular energies using the unitary coupled clus-

- ter ansatz, *Quantum Science and Technology* **4**, 014008 (2018).
- [57] B. Bauer, D. Wecker, A. J. Millis, M. B. Hastings, and M. Troyer, Hybrid quantum-classical approach to correlated materials, *Phys. Rev. X* **6**, 031045 (2016).
- [58] J. Rogers, T.-H. Lee, S. Pakdel, W. Xu, V. Dobrosavljević, Y.-X. Yao, O. Christiansen, and N. Lanatà, Bypassing the computational bottleneck of quantum-embedding theories for strong electron correlations with machine learning, *Phys. Rev. Research* **3**, 013101 (2021).

Supplemental Material: Quantum-embedding description of the Anderson lattice model with the ghost Gutzwiller Approximation

Marius S. Frank,¹ Tsung-Han Lee,² Gargee Bhattacharyya,¹ Pak Ki Henry Tsang,³
Victor Quito,^{4,3} Vladimir Dobrosavljević,³ Ove Christiansen,⁵ and Nicola Lanata^{1,6,*}

¹*Department of Physics and Astronomy, Aarhus University, 8000, Aarhus C, Denmark*

²*Physics and Astronomy Department, Rutgers University, Piscataway, New Jersey 08854, USA*

³*Department of Physics and National High Magnetic Field Laboratory,
Florida State University, Tallahassee, Florida 32306, USA*

⁴*Department of Physics and Astronomy, Iowa State University, Ames, Iowa 50011, USA*

⁵*Department of Chemistry, Aarhus University, 8000, Aarhus C, Denmark*

⁶*Nordita, KTH Royal Institute of Technology and Stockholm University, Roslagstullsbacken 23, 10691 Stockholm, Sweden*

THE g-GA THEORY

For completeness, here we provide a comprehensive derivation of the g-GA method, presenting the theory from a slightly different perspective with respect to Ref. [1] (more direct and concise, but equivalent).

The Hamiltonian

We consider a generic multi-orbital Fermionic Hamiltonian represented as follows:

$$\begin{aligned}\hat{H} &= \sum_{\mathbf{R}\mathbf{R}'} \sum_{ij} \sum_{\alpha=1}^{\nu_i} \sum_{\beta=1}^{\nu_j} t_{\mathbf{R}i,\mathbf{R}'j}^{\alpha\beta} c_{\mathbf{R}i\alpha}^\dagger c_{\mathbf{R}'j\beta} + \sum_{\mathbf{R}} \sum_{i \geq 1} \hat{H}_{\mathbf{R}i}^{\text{loc}} [c_{\mathbf{R}i\alpha}^\dagger, c_{\mathbf{R}i\alpha}] \\ &= \sum_{\mathbf{k}} \sum_{ij} \sum_{\alpha=1}^{\nu_i} \sum_{\beta=1}^{\nu_j} t_{\mathbf{k},ij}^{\alpha\beta} c_{\mathbf{k}i\alpha}^\dagger c_{\mathbf{k}j\beta} + \sum_{\mathbf{R}} \sum_{i \geq 1} \hat{H}_{\mathbf{R}i}^{\text{loc}} [c_{\mathbf{R}i\alpha}^\dagger, c_{\mathbf{R}i\alpha}],\end{aligned}\quad (1)$$

where \mathbf{R} indicates the unit-cell label, \mathbf{k} is the corresponding crystal-momentum, while i and α classify the Fermionic degrees of freedom (both spin and orbital) according to the following convention: (1) all modes with $i = 0$ are “uncorrelated”, i.e., they appear only in the quadratic part of \hat{H} (as the p modes of the ALM, introduced in the main text); (2) all modes with $i \geq 1$ are “correlated” (as the d modes of the ALM), i.e., $\hat{H}_{\mathbf{R}i}^{\text{loc}}$ are generic operators (including interaction terms) constructed from $c_{\mathbf{R}i\alpha}^\dagger c_{\mathbf{R}j\beta}$. As in the multi-orbital GA, we assume that:

$$t_{\mathbf{R}i,\mathbf{R}i}^{\alpha\beta} = 0 \quad \forall i \geq 1, \quad (2)$$

and that $\hat{H}_{\mathbf{R}i}^{\text{loc}}$ includes both the two-body local terms of the Hamiltonian and the one-body local term represented as:

$$\hat{H}_{\text{loc}}^{(1)} = \sum_{\mathbf{R}} \sum_{i \geq 1} \sum_{\alpha,\beta=1}^{\nu_i} [t_i^{\text{loc}}]_{\alpha\beta} c_{\mathbf{R}i\alpha}^\dagger c_{\mathbf{R}i\beta} = \sum_{\mathbf{k}} \sum_{i \geq 1} \sum_{\alpha,\beta=1}^{\nu_i} [t_i^{\text{loc}}]_{\alpha\beta} c_{\mathbf{k}i\alpha}^\dagger c_{\mathbf{k}i\beta}. \quad (3)$$

Note that in first-principle calculations of real materials based on density functional theory in combination with many-body techniques [2–5], such as the GA or DMFT, the solution is obtained by solving recursively multi-orbital Hamiltonian with the structure of Eq. (1) [4]. It is important to note that, within this context, the correlated degrees of freedom correspond to localized orbitals [6, 7]. Therefore, as pointed out in the conclusions of the main text, the hopping parameters between correlated and uncorrelated modes is much larger with respect to the hopping between correlated modes (as in the ALM studied in the main text). Therefore, the pathology of the GA method uncovered in this work and our observation that the g-GA extension resolves this problem are very relevant in ab-initio calculations of correlated materials.

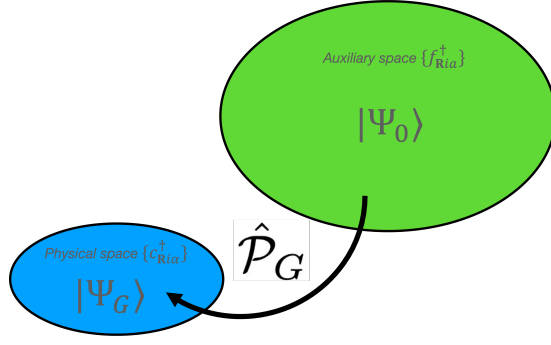


Figure 1. Schematic representation of the g-GA variational ansatz. The wavefunction $|\Psi_G\rangle$ is constructed by mapping a generic single-particle wavefunction $|\Psi_0\rangle$ constructed in an auxiliary Hilbert space, using the operator $\hat{\mathcal{P}}_G$. Both $|\Psi_0\rangle$ and $\hat{\mathcal{P}}_G$ are determined variationally

The g-GA variational ansatz

The g-GA consists in minimizing the expectation value of \hat{H} with respect to a wave function represented as follows:

$$|\Psi_G\rangle = \hat{\mathcal{P}}_G |\Psi_0\rangle \quad (4)$$

$$\hat{\mathcal{P}}_G = \prod_{i \geq 1} \hat{\mathcal{P}}_{\mathbf{R}i}, \quad (5)$$

where $|\Psi_0\rangle$ is a single-particle wavefunction constructed in an auxiliary Hilbert space, generated by $\tilde{\nu}_i > \nu_i$ degrees of freedom $f_{\mathbf{R}ia}^\dagger$ ($a = 1, \dots, \tilde{\nu}_i$) for each (\mathbf{R}, i) , while:

$$\hat{\mathcal{P}}_{\mathbf{R}i} = \sum_{\Gamma=0}^{2^{\nu_i}-1} \sum_{n=0}^{2^{\tilde{\nu}_i}-1} [\Lambda_i]_{\Gamma n} |\Gamma, \mathbf{R}i\rangle \langle n, \mathbf{R}i| \quad (6)$$

$$|\Gamma, \mathbf{R}i\rangle = [c_{\mathbf{R}i1}^\dagger]^{q_1(\Gamma)} \dots [c_{\mathbf{R}iq_{\nu_i}}^\dagger]^{q_{\nu_i}(\Gamma)} |0\rangle \quad (7)$$

$$|n, \mathbf{R}i\rangle = [f_{\mathbf{R}i1}^\dagger]^{q_1(n)} \dots [f_{\mathbf{R}iq_{\tilde{\nu}_i}}^\dagger]^{q_{\tilde{\nu}_i}(n)} |0\rangle \quad (8)$$

is an operator mapping the local auxiliary-space states into the physical space, see Fig. 1, where $q_i(j)$ represents the i -th digit of j in binary representation, and the matrix Λ_i controls how $\hat{\mathcal{P}}_{\mathbf{R}i}$ modifies the weight of the local electronic configurations. The key reason why the g-GA variational ansatz generalizes the standard multi-orbital GA theory is that $\tilde{\nu}_i > \nu_i$.

In the present work we focus on the normal phase. Note that, to enforce the condition that $|\Psi_G\rangle$ is an eigenstate of the number operator, we do *not* need to assume that $\hat{\mathcal{P}}_{\mathbf{R}i}$ commutes with the number operator, but only that:

$$\sum_{j=1}^{\tilde{\nu}_i} q_j(n) - \sum_{j=1}^{\nu_i} q_j(\Gamma) = m_i \quad \forall \Gamma, n \mid [\Lambda_i]_{\Gamma n} \neq 0, \quad (9)$$

where m_i is integer. Our choice of m_i (that, in principle, could be considered as an arbitrary variational parameter) will be specified below.

As in the standard multi-orbital GA, the variational wave function is restricted by the following conditions:

$$\langle \Psi_0 | \hat{\mathcal{P}}_{\mathbf{R}i}^\dagger \hat{\mathcal{P}}_{\mathbf{R}i} | \Psi_0 \rangle = \langle \Psi_0 | \Psi_0 \rangle = 1 \quad (10)$$

$$\langle \Psi_0 | \hat{\mathcal{P}}_{\mathbf{R}i}^\dagger \hat{\mathcal{P}}_{\mathbf{R}i} f_{\mathbf{R}ia}^\dagger f_{\mathbf{R}ib} | \Psi_0 \rangle = \langle \Psi_0 | f_{\mathbf{R}ia}^\dagger f_{\mathbf{R}ib} | \Psi_0 \rangle \quad \forall a, b = 1, \dots, \tilde{\nu}_i, \quad (11)$$

which are commonly called ‘‘Gutzwiller constraints’’. Furthermore, the so-called ‘‘Gutzwiller Approximation’’, which becomes exact in the limit of infinite coordination number [8, 9] —where Dynamical Mean Field Theory (DMFT) is exact [10]— is assumed.

The g-GA variational-energy components

As in the standard multi-orbital GA, our goal is to evaluate the variational energy:

$$\mathcal{E}(\Psi_0, \{\Lambda_i\}) = \langle \Psi_0 | \hat{\mathcal{P}}_G^\dagger \hat{H} \hat{\mathcal{P}}_G | \Psi_0 \rangle. \quad (12)$$

The only difference is that the operator $\hat{\mathcal{P}}_G^\dagger \hat{H} \hat{\mathcal{P}}_G$ and the operators appearing in Eqs. (10)-(11) reside within the auxiliary (extended) Hilbert space generated by the $f_{\mathbf{R}ia}^\dagger$ operators, where $a \in \{1, \dots, \tilde{\nu}_i\}$ and $\tilde{\nu}_i \geq \nu_i$. In fact, if we set $\tilde{\nu}_i = \nu_i$ we recover exactly the original multi-orbital GA theory.

As we explain below for completeness, all of the formal steps leading to the quantum-embedding formulation of the GA can be essentially repeated for the g-GA following Ref. [4], even if $\tilde{\nu}_i > \nu_i$. In particular, by employing the Gutzwiller approximation [8, 9] and assuming the Gutzwiller constraints [Eqs. (10),(11)], it can be shown that:

$$\langle \Psi_0 | \hat{\mathcal{P}}_G^\dagger c_{\mathbf{k}i\alpha}^\dagger c_{\mathbf{k}j\beta} \hat{\mathcal{P}}_G | \Psi_0 \rangle = \sum_{a=1}^{\tilde{\nu}_i} \sum_{b=1}^{\tilde{\nu}_j} \langle \Psi_0 | ([\mathcal{R}_i]_{a\alpha} f_{\mathbf{R}ia}^\dagger) ([\mathcal{R}_j]_{bb}^\dagger f_{\mathbf{R}'jb}) | \Psi_0 \rangle \quad \forall (\mathbf{R}, i) \neq (\mathbf{R}', j), \quad (13)$$

$$\langle \Psi_0 | \hat{\mathcal{P}}_G^\dagger \hat{H}_{\mathbf{R}i}^{\text{loc}} [c_{\mathbf{R}i\alpha}^\dagger, c_{\mathbf{R}i\alpha}] \hat{\mathcal{P}}_G | \Psi_0 \rangle = \langle \Psi_0 | \hat{\mathcal{P}}_{\mathbf{R}i}^\dagger \hat{H}_{\mathbf{R}i}^{\text{loc}} [c_{\mathbf{R}i\alpha}^\dagger, c_{\mathbf{R}i\alpha}] \hat{\mathcal{P}}_{\mathbf{R}i} | \Psi_0 \rangle, \quad (14)$$

where the $\tilde{\nu}_i \times \nu_i$ matrices \mathcal{R}_i are the solution of the following linear equation:

$$\langle \Psi_0 | \hat{\mathcal{P}}_{\mathbf{R}i}^\dagger c_{\mathbf{R}i\alpha}^\dagger \hat{\mathcal{P}}_{\mathbf{R}i} f_{\mathbf{R}ia} | \Psi_0 \rangle = \sum_{b=1}^{\tilde{\nu}_i} [\mathcal{R}_i]_{b\alpha} \langle \Psi_0 | f_{\mathbf{R}ib}^\dagger f_{\mathbf{R}ia} | \Psi_0 \rangle. \quad (15)$$

Local $|\Psi_0\rangle$ averages as a function of variational parameters

In the previous subsection we reduced the problem of evaluating the total-energy components to Eqs. (13)-(15). Since all of these equations, as well as the Gutzwiller constraints [Eqs. (10),(11)], involve expectation values with respect to $|\Psi_0\rangle$ of ‘‘local operators’’ (i.e., involving only $f_{\mathbf{R}ia}^\dagger$ and $f_{\mathbf{R}ia}$ degrees of freedom at fixed (\mathbf{R}, i)), it is useful to introduce the corresponding local reduced density matrix of $|\Psi_0\rangle$.

By exploiting the fact that $|\Psi_0\rangle$ is a single-particle wavefunction (i.e., Wick’s theorem applies to it), it can be readily verified that its reduced density matrix to the (\mathbf{R}, i) subsystem is given by:

$$\hat{P}_{\mathbf{R}i}^0 \propto \exp \left\{ - \sum_{a,b=1}^{\tilde{\nu}_i} \left[\ln \left(\frac{1 - {}^t\Delta_i}{t\Delta_i} \right) \right]_{ab} f_{\mathbf{R}ia}^\dagger f_{\mathbf{R}ib} \right\}, \quad (16)$$

where the entries of the $\tilde{\nu}_i \times \tilde{\nu}_i$ matrix Δ_i are given by:

$$[\Delta_i]_{ab} = \langle \Psi_0 | f_{\mathbf{R}ia}^\dagger f_{\mathbf{R}ib} | \Psi_0 \rangle \quad (17)$$

and ${}^t\Delta_i$ indicates the transpose of Δ_i .

From the definitions above, it can be straightforwardly verified that:

$$\langle \Psi_0 | \hat{\mathcal{P}}_{\mathbf{R}i}^\dagger \hat{\mathcal{P}}_{\mathbf{R}i} | \Psi_0 \rangle = \text{Tr} [P_i^0 \Lambda_i^\dagger \Lambda_i] \quad (18)$$

$$\langle \Psi_0 | \hat{\mathcal{P}}_{\mathbf{R}i}^\dagger \hat{\mathcal{P}}_{\mathbf{R}i} f_{\mathbf{R}ia}^\dagger f_{\mathbf{R}ib} | \Psi_0 \rangle = \text{Tr} [P_i^0 \Lambda_i^\dagger \Lambda_i \tilde{F}_{ia}^\dagger \tilde{F}_{ib}] \quad (19)$$

$$\langle \Psi_0 | \hat{\mathcal{P}}_{\mathbf{R}i}^\dagger \hat{H}_{\mathbf{R}i}^{\text{loc}} [c_{\mathbf{R}i\alpha}^\dagger, c_{\mathbf{R}i\alpha}] \hat{\mathcal{P}}_{\mathbf{R}i} | \Psi_0 \rangle = \text{Tr} [P_i^0 \Lambda_i^\dagger \hat{H}_{\mathbf{R}i}^{\text{loc}} [F_{i\alpha}^\dagger, F_{i\alpha}] \Lambda_i] \quad (20)$$

$$\langle \Psi_0 | \hat{\mathcal{P}}_{\mathbf{R}i}^\dagger c_{\mathbf{R}i\alpha}^\dagger \hat{\mathcal{P}}_{\mathbf{R}i} f_{\mathbf{R}ia} | \Psi_0 \rangle = \text{Tr} [P_i^0 \Lambda_i^\dagger F_{i\alpha}^\dagger \Lambda_i \tilde{F}_{ib}], \quad (21)$$

where Tr is the trace and:

$$[P_i^0]_{nn'} = \langle n, \mathbf{R}i | \hat{P}_{\mathbf{R}i}^0 | n', \mathbf{R}i \rangle \quad (n, n' \in \{0, \dots, 2^{\tilde{\nu}_i} - 1\}) \quad (22)$$

$$[F_{i\alpha}]_{\Gamma\Gamma'} = \langle \Gamma, \mathbf{R}i | c_{\mathbf{R}i\alpha} | \Gamma', \mathbf{R}i \rangle \quad (\Gamma, \Gamma' \in \{0, \dots, 2^{\nu_i} - 1\}) \quad (23)$$

$$[\tilde{F}_{ia}]_{nn'} = \langle n, \mathbf{R}i | f_{\mathbf{R}ia} | n', \mathbf{R}i \rangle \quad (n, n' \in \{0, \dots, 2^{\tilde{\nu}_i} - 1\}). \quad (24)$$

Matrix of slave-boson amplitudes

Following Refs. [4, 11, 12], we introduce the so-called matrix of slave-boson (SB) amplitudes [13–15]:

$$\phi_i = \Lambda_i \sqrt{P_i^0}. \quad (25)$$

By substituting Eq. (25) in Eqs. (18)-(21), it can be readily verified that the Gutzwiller constraints can be rewritten as follows:

$$\text{Tr}[\phi_i^\dagger \phi_i] = \langle \Psi_0 | \Psi_0 \rangle = 1 \quad (26)$$

$$\text{Tr}[\phi_i^\dagger \phi_i \tilde{F}_{ia}^\dagger \tilde{F}_{ib}] = \langle \Psi_0 | f_{\mathbf{R}ia}^\dagger f_{\mathbf{R}ib} | \Psi_0 \rangle = [\Delta_i]_{ab} \quad \forall a, b = 1, \dots, \tilde{\nu}_i \quad (27)$$

and that Eq. (15) can be rewritten as follows:

$$\text{Tr}[\phi_i^\dagger F_{i\alpha}^\dagger \phi_i \tilde{F}_{ia}] = \sum_{c=1}^{\tilde{\nu}_i} [\mathcal{R}_i]_{c\alpha} [\Delta_i (1 - \Delta_i)]_{ca}^{\frac{1}{2}}. \quad (28)$$

Embedding mapping

Following Ref. [4], we introduce the so called “embedding states,” which are related to the SB amplitudes as follows:

$$|\Phi_i\rangle = \sum_{\Gamma=0}^{2^{\nu_i}-1} \sum_{n=0}^{2^{\tilde{\nu}_i}-1} e^{i\frac{\pi}{2}N(n)(N(n)-1)} [\phi_i]_{\Gamma n} |\Gamma; i\rangle \otimes U_{\text{PH}}|n; i\rangle \quad (29)$$

where

$$|\Gamma; i\rangle = [\hat{c}_{i1}^\dagger]^{q_1(\Gamma)} \dots [\hat{c}_{iq_{\tilde{\nu}_i}}^\dagger]^{q_{\nu_i}(\Gamma)} |0\rangle \quad (30)$$

$$|n; i\rangle = [\hat{f}_{i1}^\dagger]^{q_1(n)} \dots [\hat{f}_{iq_{\tilde{\nu}_i}}^\dagger]^{q_{\tilde{\nu}_i}(n)} |0\rangle, \quad (31)$$

U_{PH} is a particle-hole transformation acting over the $|n; i\rangle$ states and

$$N(n) = \sum_{a=1}^{\tilde{\nu}_i} q_a(n). \quad (32)$$

Note that the set of all embedding states represented as in Eq. (29) constitute a Fock space, corresponding to an “impurity” (generated by the Fermionic degrees of freedom $\hat{c}_{i\alpha}$, $\alpha \in \{1, \dots, \nu_i\}$) and a “bath” (generated by the Fermionic degrees of freedom \hat{f}_{ia} , $a \in \{1, \dots, \tilde{\nu}_i\}$).

The case $B = 1$ corresponds to the standard GA theory, where the bath has the same size of the impurity. In the present work we assumed that $\tilde{\nu}_i = B\nu_i$ and set $B = 3$, see Fig. 2. Furthermore, we set $m_i = (\tilde{\nu}_i - \nu_i)/2 = 2$ (see Eq. (9)). Note that, from the definitions [Eqs. (25),(29)], it follows that this is equivalent to assume that $|\Phi_i\rangle$ has a total of $(\tilde{\nu}_i + \nu_i)/2 = 4$ electrons (i.e., that the embedding states are half-filled).

It can be readily verified by inspection that the Gutzwiller constraints can be rewritten as follows:

$$\langle \Phi_i | \Phi_i \rangle = \langle \Psi_0 | \Psi_0 \rangle = 1 \quad (33)$$

$$\langle \Phi_i | \hat{f}_{ib} \hat{f}_{ia}^\dagger | \Phi_i \rangle = \langle \Psi_0 | f_{\mathbf{R}ia}^\dagger f_{\mathbf{R}ib} | \Psi_0 \rangle = [\Delta_i]_{ab} \quad \forall a, b = 1, \dots, \tilde{\nu}_i, \quad (34)$$

the expectation value of the local terms of \hat{H} can be calculated as:

$$\langle \Psi_0 | \hat{\mathcal{P}}_{\mathbf{R}i}^\dagger \hat{H}_{\mathbf{R}i}^{\text{loc}} [c_{\mathbf{R}i\alpha}^\dagger, c_{\mathbf{R}i\alpha}] \hat{\mathcal{P}}_{\mathbf{R}i} | \Psi_0 \rangle = \langle \Phi_i | \hat{H}_{\mathbf{R}i}^{\text{loc}} [\hat{c}_{i\alpha}^\dagger, \hat{c}_{i\alpha}] | \Phi_i \rangle \quad (35)$$

and that Eq. (15) can be rewritten as:

$$\langle \Psi_0 | \hat{c}_{i\alpha}^\dagger \hat{f}_{ia}^\dagger | \Psi_0 \rangle = \sum_{c=1}^{\tilde{\nu}_i} [\mathcal{R}_i]_{c\alpha} [\Delta_i (1 - \Delta_i)]_{ca}^{\frac{1}{2}}. \quad (36)$$

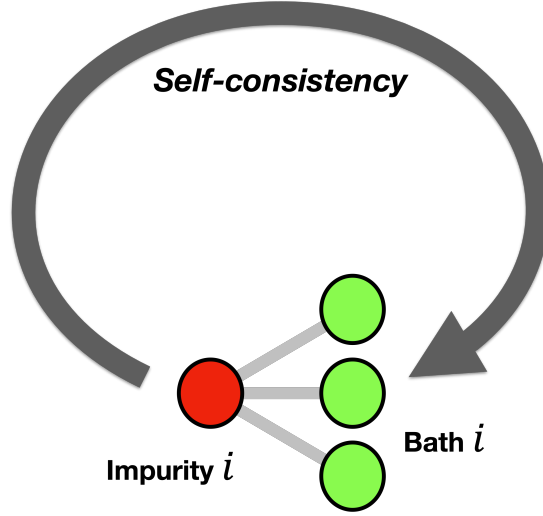


Figure 2. Schematic representation of the quantum-embedding algorithmic structure of the g-GA method. Here the number of bath sites $B = \tilde{\nu}_i/\nu_i$ (green circles) in the embedding Hamiltonian is set to 3 (as in the calculations of the main text).

In summary, by substituting Eqs. (13) and (14) in Eq. (12) and using the equations above, we deduce that the goal is to minimize the following expression for the variational energy:

$$\mathcal{E} = \sum_{\mathbf{R}\mathbf{R}'} \sum_{i,j \geq 0} \sum_{a,b=1}^{\tilde{\nu}_i} \left[\mathcal{R}_i t_{\mathbf{R}i, \mathbf{R}'j} \mathcal{R}_j^\dagger \right]_{ab} f_{\mathbf{R}ia}^\dagger f_{\mathbf{R}'jb} + \sum_{\mathbf{R}} \sum_{i \geq 1} \langle \Phi_i | \hat{H}_{\mathbf{R}i}^{\text{loc}} [\hat{c}_{i\alpha}^\dagger, \hat{c}_{i\alpha}] | \Phi_i \rangle \quad (37)$$

while fulfilling the Gutzwiller constraints [Eqs. (33), (34)].

Lagrange formulation of the g-GA

Following Refs. 1, 4, and 15, the constrained energy-minimization problem described above can be cast in terms of the following Lagrange function:

$$\begin{aligned} \mathcal{L}[\Phi, E^c; \mathcal{R}, \lambda; \mathcal{D}, \lambda^c; \Delta, \Psi_0, E] &= \frac{1}{\mathcal{N}} \langle \Psi_0 | \hat{H}_{\text{qp}}[\mathcal{R}, \lambda] | \Psi_0 \rangle + E(1 - \langle \Psi_0 | \Psi_0 \rangle) \\ &+ \sum_{i \geq 1} \left[\langle \Phi_i | \hat{H}_i^{\text{emb}}[\mathcal{D}_i, \lambda_i^c] | \Phi_i \rangle + E_i^c(1 - \langle \Phi_i | \Phi_i \rangle) \right] \\ &- \sum_{i \geq 1} \left[\sum_{a,b=1}^{\tilde{\nu}_i} ([\lambda_i]_{ab} + [\lambda_i^c]_{ab}) [\Delta_i]_{ab} + \sum_{c,a=1}^{\tilde{\nu}_i} \sum_{\alpha=1}^{\nu_i} ([\mathcal{D}_i]_{a\alpha} [\mathcal{R}_i]_{c\alpha} [\Delta_i(1 - \Delta_i)]_{ca}^{\frac{1}{2}} + \text{c.c.}) \right], \quad (38) \end{aligned}$$

where \mathcal{N} is the total number of unit cells, E and E^c are real numbers, Δ_i , λ_i^c and λ_i are $\tilde{\nu}_i \times \tilde{\nu}_i$ Hermitian matrices, \mathcal{D}_i and \mathcal{R}_i are generic (rectangular) $\tilde{\nu}_i \times \nu_i$ matrices. The auxiliary Hamiltonians \hat{H}_{qp} and \hat{H}_{emb} , which are called “quasiparticle Hamiltonian” and “Embedding Hamiltonian,” respectively, are defined as follows:

$$\hat{H}_{\text{qp}} = \sum_{\mathbf{R}\mathbf{R}'} \sum_{i,j \geq 0} \sum_{a,b=1}^{\tilde{\nu}_i} \left[\mathcal{R}_i t_{\mathbf{R}i, \mathbf{R}'j} \mathcal{R}_j^\dagger \right]_{ab} f_{\mathbf{R}ia}^\dagger f_{\mathbf{R}'jb} + \sum_{\mathbf{R}} \sum_{i \geq 0} \sum_{a,b=1}^{\tilde{\nu}_i} [\lambda_i]_{ab} f_{\mathbf{R}ia}^\dagger f_{\mathbf{R}ib} \quad (39)$$

$$\hat{H}_i^{\text{emb}} = \hat{H}_i^{\text{loc}} [\{\hat{c}_i^\dagger, \hat{c}_i\}] + \sum_{a=1}^{\tilde{\nu}_i} \sum_{\alpha=1}^{\nu_i} [\mathcal{D}_i]_{a\alpha} \hat{c}_{i\alpha}^\dagger \hat{f}_{ia} + \sum_{a,b=1}^{\tilde{\nu}_i} [\lambda_i^c]_{ab} \hat{f}_{ib} \hat{f}_{ia}^\dagger \quad \forall i \geq 1. \quad (40)$$

The saddle-point of the Lagrangian \mathcal{L} defined in Eq. (38) is given by the following equations:

$$\frac{1}{\mathcal{N}} \left[\sum_{\mathbf{k}} \Pi_i f(\mathcal{R} t_{\mathbf{k}} \mathcal{R}^\dagger + \lambda) \Pi_i \right]_{ba} = [\Delta_i]_{ab} \quad (41)$$

$$\frac{1}{\mathcal{N}} \left[\sum_{\mathbf{k}} \Pi_i t_{\mathbf{k}} \mathcal{R}^\dagger f(\mathcal{R} t_{\mathbf{k}} \mathcal{R}^\dagger + \lambda) \Pi_i \right]_{\alpha\alpha} = \sum_{c,a=1}^{\tilde{\nu}_i} \sum_{\alpha=1}^{\nu_i} [\mathcal{D}_i]_{c\alpha} [\Delta_i (1 - \Delta_i)]^{\frac{1}{2}} \quad (42)$$

$$\sum_{c,b=1}^{\tilde{\nu}_i} \sum_{\alpha=1}^{\nu_i} \frac{\partial}{\partial [d_i^0]_s} \left([\Delta_i (1 - \Delta_i)]_{cb}^{\frac{1}{2}} [\mathcal{D}_i]_{b\alpha} [\mathcal{R}_i]_{c\alpha} + \text{c.c.} \right) + [l_i + l_i^c]_s = 0 \quad (43)$$

$$\hat{H}_i^{\text{emb}} |\Phi_i\rangle = E_i^c |\Phi_i\rangle \quad (44)$$

$$[\mathcal{F}_i^{(1)}]_{\alpha\alpha} = \langle \Phi_i | \hat{c}_{i\alpha}^\dagger \hat{f}_{ia} | \Phi_i \rangle - \sum_{c=1} [\Delta_i (1 - \Delta_i)]^{\frac{1}{2}} [\mathcal{R}_i]_{c\alpha} \stackrel{!}{=} 0 \quad (45)$$

$$[\mathcal{F}_i^{(2)}]_{ab} = \langle \Phi_i | \hat{f}_{ib} \hat{f}_{ia}^\dagger | \Phi_i \rangle - [\Delta_i]_{ab} \stackrel{!}{=} 0, \quad (46)$$

where f is the zero-temperature Fermi function and in Eqs. (41),(42) we introduced the following block-matrices:

$$\lambda = \begin{pmatrix} [\mathbf{0}]_{\nu_0 \times \nu_0} & \cdots & \cdots & \mathbf{0} \\ \vdots & \lambda_1 & \vdots & \\ \vdots & \vdots & \ddots & \vdots \\ \mathbf{0} & \cdots & \cdots & \lambda_M \end{pmatrix}, \quad (47)$$

$$\mathcal{R} = \begin{pmatrix} [\mathbf{1}]_{\nu_0 \times \nu_0} & \cdots & \cdots & \mathbf{0} \\ \mathbf{0} & \mathcal{R}_1 & \cdots & \vdots \\ \vdots & \vdots & \ddots & \vdots \\ \mathbf{0} & \cdots & \cdots & \mathcal{R}_M \end{pmatrix}, \quad (48)$$

where $[\mathbf{1}]_{n \times n}$ is the $n \times n$ identity matrix and $[\mathbf{0}]_{n \times n}$ is the $n \times n$ zero matrix. We also introduced the following projectors:

$$\Pi_i = \begin{pmatrix} \delta_{i0} [\mathbf{1}]_{\nu_0 \times \nu_0} & \cdots & \cdots & \mathbf{0} \\ \vdots & \delta_{i1} [\mathbf{1}]_{\tilde{\nu}_1 \times \tilde{\nu}_1} & \cdots & \vdots \\ \vdots & \vdots & \ddots & \vdots \\ \mathbf{0} & \cdots & \cdots & \delta_{iM} [\mathbf{1}]_{\tilde{\nu}_M \times \tilde{\nu}_M} \end{pmatrix}. \quad (49)$$

Finally, we introduced the following expansions of the matrices Δ_i , λ_i , λ_i^c , in terms of an orthonormal basis of Hermitian matrices $\{[h_i]_s\}$ (with respect to the canonical scalar product $(A, B) = \text{Tr}[A^\dagger B]$):

$$\Delta_i = \sum_{s=1}^{\tilde{\nu}_i^2} [d_i^0]_s {}^t [h_i]_s \quad (50)$$

$$\lambda_i = \sum_{s=1}^{\tilde{\nu}_i^2} [l_i]_s [h_i]_s \quad (51)$$

$$\lambda_i^c = \sum_{s=1}^{\tilde{\nu}_i^2} [l_i^c]_s [h_i]_s, \quad (52)$$

where $[d_i^0]_s$, $[l_i]_s$ and $[l_i^c]_s$ are real-valued coefficients.

Algorithmic structure of the g-GA

The equations (41)-(46) can be solved numerically using the following numerical procedure (represented schematically in Fig. 2):

1. Starting from an initial guess for the coefficients $[r_i]_a$ and $[l_i]_s$ construct the matrix \mathcal{R}_i directly by using $[r_i]_a$ as the matrix elements of \mathcal{R}_i and the matrix λ_i according to Eq. (51).
2. Arrange the \mathcal{R}_i and λ_i in block matrices over all i as shown in Eqs. (47) and (48) and construct \hat{H}_{qp} as shown in Eq.(39).
3. Compute Δ_i according to Eq. (41) using the projector Π_i as given in Eq. (49).
4. Compute the Lagrange multipliers \mathcal{D}_i by inverting Eq. (42).
5. Determine the coefficients $[l_i^c]_s$ from Eq. (43) and construct the matrix λ_i^c according to Eq. (52).
6. Construct \hat{H}_i^{emb} according to Eq. (40) and calculate its ground state $|\Phi_i\rangle$ within the subspace with $(\nu_i + \tilde{\nu}_i)/2$ electrons (i.e., half of the total number of EH modes).
7. Compute $\mathcal{F}_i^{(1)}$ and $\mathcal{F}_i^{(2)}$ according to equations (45) and (46).

A saddle-point of \mathcal{L} satisfies $\mathcal{F}_i^{(1)} = \mathcal{F}_i^{(2)} = 0$, i.e., the procedure described above has to be repeated until a self-consistent solution to these equations is found.

Gauge invariance of the g-GA

Following Ref. 15 it can be readily shown that also the g-GA Lagrangian is invariant with respect to the following Gauge transformation:

$$|\Psi_0\rangle \rightarrow \mathcal{U}^\dagger(\theta) |\Psi_0\rangle \quad (53)$$

$$|\Phi_i\rangle \rightarrow U_i^\dagger(\theta_i) |\Phi_i\rangle \quad (54)$$

$$\mathcal{R}_i \rightarrow u_i^\dagger(\theta_i) \mathcal{R}_i \quad (55)$$

$$\mathcal{D}_i \rightarrow {}^t u(\theta_i) \mathcal{D}_i \quad (56)$$

$$\Delta_i \rightarrow {}^t u_i(\theta_i) \Delta_i {}^t u_i^\dagger(\theta_i) \quad (57)$$

$$\lambda_i \rightarrow u_i^\dagger(\theta_i) \lambda_i u_i(\theta_i) \quad (58)$$

$$\lambda_i^c \rightarrow u_i^\dagger(\theta_i) \lambda_i^c u_i(\theta_i) , \quad (59)$$

with:

$$u_i(\theta_i) = e^{i\theta_i} \quad (60)$$

$$U_i(\theta_i) = e^{i \sum_{a,b=1}^{\tilde{\nu}_i} [\theta_i]_{ab} \hat{f}_{ia}^\dagger \hat{f}_{ib}} \quad (61)$$

$$\mathcal{U}(\theta) = e^{i \sum_R \sum_{i \geq 1} \sum_{a,b=1}^{\tilde{\nu}_i} [\theta_i]_{ab} \hat{f}_{Ria}^\dagger \hat{f}_{Rib}} , \quad (62)$$

where $u_i(\theta_i) \in \mathbb{C}^{\tilde{\nu}_i \times \tilde{\nu}_i}$, $U_i(\theta_i) \in \mathbb{C}^{2\tilde{\nu}_i \times 2\tilde{\nu}_i}$ and $\mathcal{U}(\theta) \in \mathbb{C}^{2\tilde{\nu} \times 2\tilde{\nu}}$ and θ_i are Hermitian matrices.

General analytical expression for spectral function from g-GA variational parameters

Let us consider the g-GA zero-temperature spectral function, defined as follows:

$$\mathcal{A}_{i\alpha,j\beta}(\mathbf{k}, \omega) = \langle \Psi_G | c_{\mathbf{k}i\alpha} \delta(\omega - \hat{H}) c_{\mathbf{k}j\beta}^\dagger | \Psi_G \rangle + \langle \Psi_G | c_{\mathbf{k}j\beta}^\dagger \delta(\omega + \hat{H}) c_{\mathbf{k}i\alpha} | \Psi_G \rangle . \quad (63)$$

Following Ref. 1, we obtain the following approximation to the physical Green's function:

$$\mathcal{G}_{i\alpha,j\beta}(\mathbf{k}, \omega) = \int_{-\infty}^{\infty} d\epsilon \frac{\mathcal{A}_{i\alpha,j\beta}(\mathbf{k}, \omega)}{\omega - \epsilon} \simeq \left[\mathcal{R}_i^\dagger \Pi_i \frac{1}{\omega - [\mathcal{R}\epsilon_{\mathbf{k}}\mathcal{R}^\dagger + \lambda]} \Pi_j \mathcal{R}_j \right]_{\alpha\beta} . \quad (64)$$

As explained above, the g-GA Lagrange function is invariant under the group of gauge transformations defined by Eqs. (53)-(59). To calculate the self-energy, it is convenient to choose a gauge such that λ_i is diagonal and decompose R_i and λ_i as follows:

$$\mathcal{R}_i = \begin{pmatrix} \mathcal{R}_i^{(1)} \\ \mathcal{R}_i^{(2)} \end{pmatrix} \quad (65)$$

$$\lambda_i = \begin{pmatrix} \lambda_i^{(1)} & \mathbf{0} \\ \mathbf{0} & \lambda_i^{(2)} \end{pmatrix}, \quad (66)$$

where $\mathcal{R}_i^{(1)}$ and $\lambda_i^{(1)}$ are matrices of dimension $\nu_i \times \nu_i$, while $\mathcal{R}_i^{(2)}$ and $\lambda_i^{(2)}$ are $(\tilde{\nu}_i - \nu_i) \times \nu_i$ and $(\tilde{\nu}_i - \nu_i) \times (\tilde{\nu}_i - \nu_i)$, respectively. In this gauge, using Eqs. (65), (66) and the Dyson equation:

$$\mathcal{G}(\mathbf{k}, \omega) = [\omega - \tau_{\mathbf{k}} - \Sigma(\omega)]^{-1} \quad (67)$$

(where $\tau_{\mathbf{k}} = t_{\mathbf{k}} + t^{\text{loc}}$ also contains all local terms of Eq. (3)), it can be shown with a straightforward calculation that the self-energy is given by the following equation:

$$\Sigma(\omega) = \begin{pmatrix} [\mathbf{0}]_{\nu_0 \times \nu_0} & \mathbf{0} & \dots & \mathbf{0} \\ \mathbf{0} & \Sigma_1(\omega) & \dots & \vdots \\ \vdots & \vdots & \ddots & \vdots \\ \mathbf{0} & \dots & \dots & \Sigma_M(\omega) \end{pmatrix}, \quad (68)$$

where, as expected, $\Sigma(\omega)$ is local (\mathbf{k} -independent) and $\Sigma_i(\omega)$ are the $\nu_i \times \nu_i$ matrices $\forall i \geq 1$, given by the following equation:

$$\begin{aligned} \Sigma_i(\omega) = & t_i^{\text{loc}} - \omega \frac{\mathbf{1} - \mathcal{R}_i^{(1)\dagger} \mathcal{R}_i^{(1)}}{\mathcal{R}_i^{(1)\dagger} \mathcal{R}_i^{(1)}} + [\mathcal{R}_i^{(1)}]^{-1} \lambda_i^{(1)} [\mathcal{R}_i^{(1)\dagger}]^{-1} + [\mathcal{R}_i^{(1)}]^{-1} (\omega - \lambda_i^{(1)}) [\mathcal{R}_i^{(1)\dagger}]^{-1} \mathcal{R}_i^{(2)\dagger} \\ & \times \left[\mathcal{R}_i^{(2)} [\mathcal{R}_i^{(1)}]^{-1} (\omega - \lambda_i^{(1)}) [\mathcal{R}_i^{(1)\dagger}]^{-1} \mathcal{R}_i^{(2)\dagger} + (\omega - \lambda_i^{(2)}) \right]^{-1} \\ & \times \mathcal{R}_i^{(2)} [\mathcal{R}_i^{(1)}]^{-1} (\omega - \lambda_i^{(1)}) [\mathcal{R}_i^{(1)\dagger}]^{-1}, \end{aligned} \quad (69)$$

which reduces to Eq. 10 of the main text for single-orbital impurities.

Note that, as pointed out in the main text, from Eq. (64) it follows that the poles of the Green's function lie on top of the eigenvalues of the quasi-particle Hamiltonian, see Eq. (39). However, because of the matrices \mathcal{R}_i^\dagger and \mathcal{R}_j at the left and the right of Eq. (64) —which are rectangular, — only a portion of the quasi-particle spectral weight is physical (see Fig. 3 of the main text).

PATHOLOGY OF THE BARE GA IN THE NARROW-BANDWIDTH LIMIT OF THE ALM

As pointed out in the main text, within the GA the Mott transition of the ALM occurs (by construction) only when $\langle d_{i\sigma}^\dagger p_{i\sigma} \rangle_{\text{GA}} = r \langle \Psi_0 | f_{i\sigma}^\dagger p_{i\sigma} | \Psi_0 \rangle = 0$, i.e., when the variational parameter r vanishes. However, as shown in Fig. 1 of the main text, the GA critical value U_c is overestimated dramatically for the ALM, especially for $\epsilon_p \ll -1$.

To explain this behavior, it is insightful to inspect the GA solution also in the narrow-bandwidth limit, i.e., setting the half-bandwidth W of the Bethe-lattice hopping matrix to 0 —corresponding to a series of decoupled p - d dimers. The resulting evolution of U_c (i.e., the interaction strength such that r vanishes) is shown here in Fig. 3, where we set $V = 1$ and consider $\epsilon_p \ll -1$.

We observe that, not surprisingly (since $V = 1$), $\langle d_{i\sigma}^\dagger p_{i\sigma} \rangle_{\text{GA}}$ does not vanish at $U \sim 0$ (neither for $W = 0$ nor for $W = 1$). In fact, at $U = 0$ the GA wavefunction is exact. On the other hand, in this limit any infinitesimal U should induce a Mott transition for $W \rightarrow 0$. This simple observation showcases very clearly how, as pointed out in the main text, the p - d charge fluctuations cannot be neglected in the Mott phase —as they *must* coexist in the narrow-bandwidth limit of the ALM. In other words, the argument above shows that —for small W — the GA behavior of

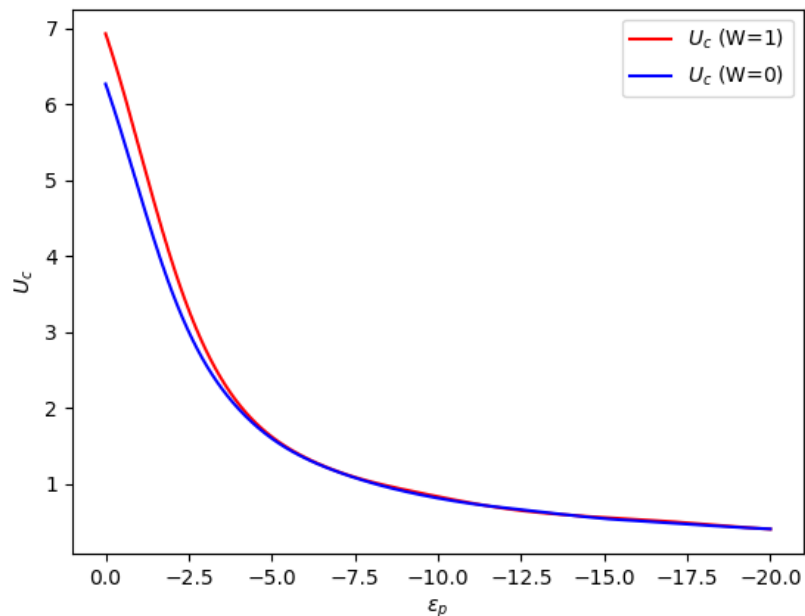


Figure 3. Behavior of U_c as a function of ϵ_p in bare GA for $V = 1$, both for $W = 1$ (red) and in the narrow-bandwidth limit $W = 0$ (blue).

U_c is essentially unrelated with the Mott transition. We also note that, for the values of ϵ_p considered in Fig. 3, the GA behavior of U_c is almost independent of whether $W = 0$ or $W = 1$. In fact, one can readily demonstrate also analytically that the bare GA predicts that $U_c(W) \sim U_c(W = 0) \sim V^2/|\epsilon_p| \forall W$ for $\epsilon_p \rightarrow -\infty$ (which is clearly incorrect). This shows that the pathology of the GA, that we discussed above in the narrow-bandwidth limit, cannot be only regarded as an accident specific to this particular case, as it affects the GA predictions also for finite W .

In summary, while the bare GA captures some qualitative features of the phase diagram of the ALM, here we identified a pathological behavior of this method in the narrow-bandwidth limit, which leads to a dramatic overestimation of U_c (especially for $\epsilon_p \rightarrow -\infty$). From a general perspective, this problem can be traced back to the inability of the GA of describing simultaneously the Mott physics and the p - d charge fluctuations. In the main text we showed that the g-GA does not have such limitation and, consequently, it resolves the problems of the bare GA here uncovered, providing us with a description of the ALM with accuracy comparable to DMFT.

* Corresponding author: lanata@phys.au.dk

- [1] N. Lanatà, T.-H. Lee, Y.-X. Yao, and V. Dobrosavljević, Emergent Bloch excitations in Mott matter, *Phys. Rev. B* **96**, 195126 (2017).
- [2] V. I. Anisimov, A. I. Oteryaev, M. A. Korotin, A. O. Anokhin, and G. Kotliar, First-principles calculations of the electronic structure and spectra of strongly correlated systems: dynamical mean-field theory, *J. Phys. Condens. Matter* **9**, 7359 (1997).
- [3] X.-Y. Deng, L. Wang, X. Dai, and Z. Fang, Local density approximation combined with Gutzwiller method for correlated electron systems: Formalism and applications, *Phys. Rev. B* **79**, 075114 (2009).
- [4] N. Lanatà, Y.-X. Yao, C.-Z. Wang, K.-M. Ho, and G. Kotliar, Phase diagram and electronic structure of praseodymium and plutonium, *Phys. Rev. X* **5**, 011008 (2015).
- [5] V. I. Anisimov, F. Aryasetiawan, and A. I. Lichtenstein, First-principles calculations of the electronic structure and spectra of strongly correlated systems: the LDA+U method, *J. Phys. Condens. Matter* **9**, 767 (1997).
- [6] K. Haule, C.-H. Yee, and K. Kim, Dynamical mean-field theory within the full-potential methods: Electronic structure of CeIrIn₅, CeCoIn₅, and CeRhIn₅, *Phys. Rev. B* **81**, 195107 (2010).
- [7] F. Lechermann, A. Georges, A. Poteryaev, S. Biermann, M. Posternak, A. Yamasaki, and O. K. Andersen, Dynamical mean-field theory using Wannier functions: A flexible route to electronic structure calculations of strongly correlated materials, *Phys. Rev. B* **74**, 125120 (2006).
- [8] M. C. Gutzwiller, Correlation of Electrons in a Narrow s Band, *Phys. Rev.* **137**, A1726 (1965).
- [9] W. Metzner and D. Vollhardt, Correlated lattice fermions in $d = \infty$ dimensions, *Phys. Rev. Lett.* **62**, 324 (1989).

- [10] A. Georges, G. Kotliar, W. Krauth, and M. J. Rozenberg, Dynamical mean-field theory of strongly correlated fermion systems and the limit of infinite dimensions, *Rev. Mod. Phys.* **68**, 13 (1996).
- [11] N. Lanatà, P. Barone, and M. Fabrizio, Fermi-surface evolution across the magnetic phase transition in the Kondo lattice model, *Phys. Rev. B* **78**, 155127 (2008).
- [12] J. Bünemann and F. Gebhard, Equivalence of Gutzwiller and slave-boson mean-field theories for multiband Hubbard models, *Phys. Rev. B* **76**, 193104 (2007).
- [13] R. Frésard and P. Wölfle, Unified slave boson representation of spin and charge degrees of freedom for strongly correlated fermi systems, *International Journal of Modern Physics B* **06**, 685 (1992).
- [14] F. Lechermann, A. Georges, G. Kotliar, and O. Parcollet, Rotationally invariant slave-boson formalism and momentum dependence of the quasiparticle weight, *Phys. Rev. B* **76**, 155102 (2007).
- [15] N. Lanatà, Y.-X. Yao, X. Deng, V. Dobrosavljević, and G. Kotliar, Slave Boson Theory of Orbital Differentiation with Crystal Field Effects: Application to UO_2 , *Phys. Rev. Lett.* **118**, 126401 (2017).